# Electronic Supplementary Information (ESI)

## A highly efficient and stable solar energy-driven device using lignocellulosic biomass *Juncus effusus* for the recovery of ethanol-water mixture

Zhuan Fu,‡[a,b] Sijie Zhou,‡[a,c] Liangjun Xia,*[a,d] Chunhua Zhang,[a] Na Zhu,[a] Junyao Gong,[a] Xiaofeng Wang,[a] Xin Liu,[a] Li Li,*[d] and Weilin Xu*[a]

[a] State Key Laboratory of New Textile Materials and Advanced Processing Technologies, Wuhan Textile University, Wuhan 430200, China.

[b] College of Textile Science and Engineering, Zhejiang Sci-Tech University, Hangzhou 310018, China.

[c] College of Textiles, Donghua University, Shanghai 201620, China.

[d] Institute of Textiles and Clothing, The Hong Kong Polytechnic University, Hong Kong 999077, China.

* Corresponding authors.

E-mail addresses: liangjun_xia@hotmail.com (L. Xia), li.lilly@polyu.edu.hk (L. Li), weilin_xu0@163.com (W. Xu).

‡ These authors contributed equally to this work.

## Indoor Solar Distillation

The alcohol-water mixture was contained in a plastic vessel (length: width: height= 6 cm: 6 cm: 5.5 cm). An Expandable Polyethylene foam tank (1.9 cm thick) was used as a thermally insulating layer and helped the *x*-SA to float in the aqueous ethanol solution. The solar absorber contacted the solution through a square hole (3cm × 3cm) in the bottom of the foam trough and wicked the solution up (refer to Fig. 4a for details). Subsequently, the solar evaporation experiments were performed under AM 1.5G simulated irradiation. The solar-powered steam generation experiments were carried out in the laboratory environment at a temperature of ~22°C and a humidity of ~60%.

For the purification of dye effluent, kinds of dye effluent samples were prepared by dissolving different colored reactive dyes (50 mg/L RR195, RY145, and RB222) in an EtOH-$H_2O$ mixture (90/10, v/v). The dyeing method of the EtOH-$H_2O$ system has been studied in detail in previous papers.[1, 2] Moreover, a sphere-like apparatus for evaporation and condensation was constructed to collect the clean EtOH-$H_2O$ mixture.

## Field Solar Dye Effluent Purification on Rooftop

For the practical solar dye effluent treatment, a large 1-SA (30 cm × 30 cm) was prepared and a single-slope quartz glass solar distiller was designed (Fig. S19). The tilt angle of the condensation cover was set at 45°. The simulated dye effluent was produced by dissolving 50 mg/L of the reactive red dye (RR195) in the EtOH-$H_2O$ mixture, in which the volume ratio of ethanol to water was 90:10. The devices were placed at the Wuhan Textile University campus (north latitude 30°) from 10:00 to 18:00 each day, and the weather conditions and the collection of the clean EtOH-$H_2O$ mixture were recorded. At the same time, the solar flux per hour during the test period was recorded and the daily average was calculated.

## Measurement of specific heat capacity

Based on the sapphire method, the specific heat capacity of samples was measured and calculated from their DSC spectra. In this method, the heat flow was measured through three separate aluminum crucibles, filled with sapphire, sample, and empty, respectively. Subsequently, combining the three results, the specific heat capacity of the sample can be calculated by the equation:

$$C = \frac{(D - De) \cdot ms}{(Ds - De) \cdot m} \cdot Cs$$

where $C$ and $C_s$ are the specific heat capacities of the sample and sapphire, respectively. $m$ and $m_s$ refer to the weights of sample and sapphire, respectively. $D$, $D_{s,}$ and $D_e$ represent the DSC values of aluminum crucibles containing sample, sapphire, and empty, respectively.

## Calculation of solar absorption of the materials

The ultraviolet-visible-near infrared (UV-vis-NIR) diffuse reflectance spectrum of the sample was measured (Fig. S6), after which the absorbance of the sample was calculated by the equation:[3, 4]

$$A = \frac{\int (1 - R) \cdot S \cdot d\lambda}{\int S \cdot d\lambda}$$

where $A$ is the solar absorption of the sample, $R$ is the reflectance, $S$ is the solar irradiance (W $m^{-2}$ $nm^{-1}$), $\lambda$ is the wavelength (nm) and $(1-R)\cdot S$ represents the sample absorption of the solar irradiance.

## Thermal Conductivity Measurement

Based on published research,[5-7] the thermal conductivity of wet samples was measured by a self-built device using the steady-state method (Fig. S8a). The sample was sandwiched between two pieces of glass, and the top glass was covered with a layer of black tape. A xenon lamp was used as the heat source at the top, and the ice at the bottom was used to dissipate the heat. An infrared (IR) camera was utilized to monitor the temperature distribution of the sample sides (Fig. S8b and c). Fourier equation was used to calculate the thermal conductivity of each sample:

$$q = -k\frac{dT}{dx} = -k\frac{T2 - T1}{d1}$$

where the thermal conductivity $k$ of the glass is known to be 1.0 W $m^{-1}$ $K^{-1}$,[8, 9] $T_1$ and $T_2$ are the temperatures at the interfaces of $I_1$ and $I_2$, respectively, and d1 is the thickness of the glass (4.5 mm). After obtaining the heat flux $q$, the thermal conductivity of the sample can be obtained from the equation:

$$k = -q\frac{dx}{dT} = -q\frac{d2}{T3 - T2}$$

where $k$ is the thermal conductivity of the test sample, $T_3$ is the temperature at the $I_3$ interface, $d_2$ is the thickness of the sample (3 mm).

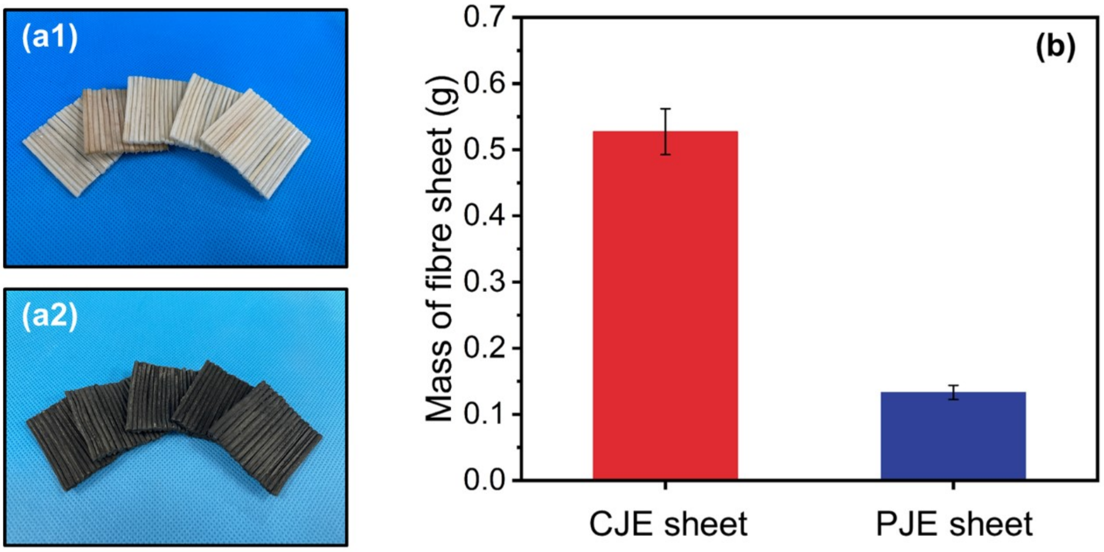

**Fig. S1** Photographs of (a1) PJE sheets and (a2) CJE sheets. (b) Average mass of CJE sheets and PJE sheets.

The average mass of the PJE sheets and CJE sheets was 0.13 g and 0.53 g, respectively. The difference between the two sheets was used to calculate the loading of CNTs in the CJE sheets, which was nearly 0.75 g/g.

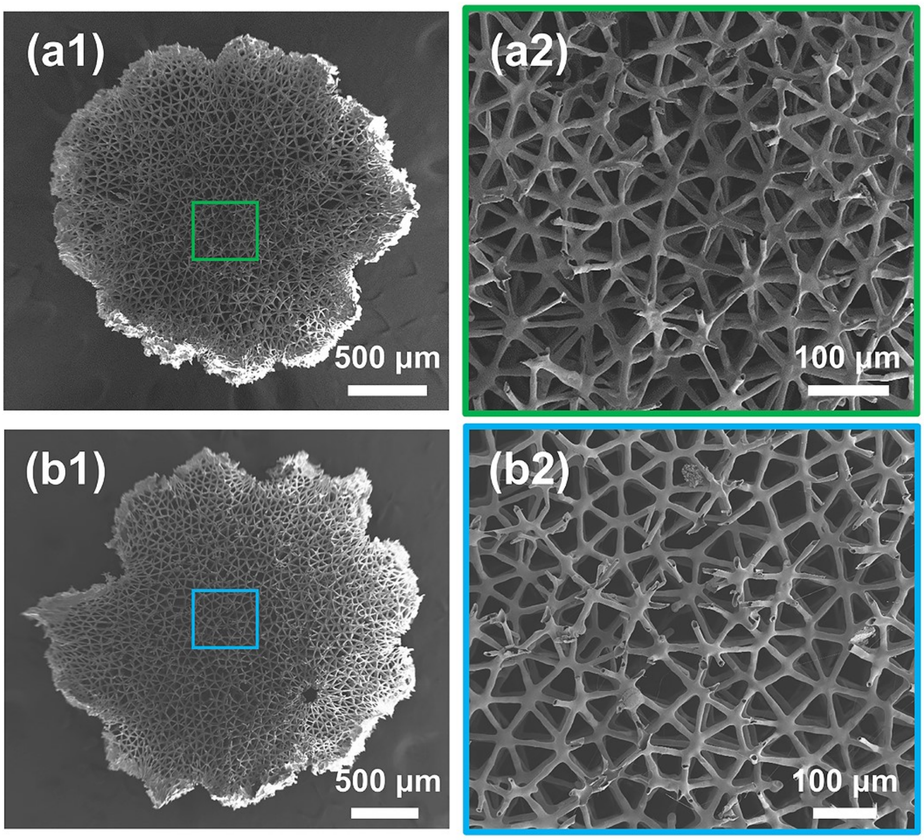

**Fig. S2** The cross-section view of (a) JE and (b) PJE, respectively.

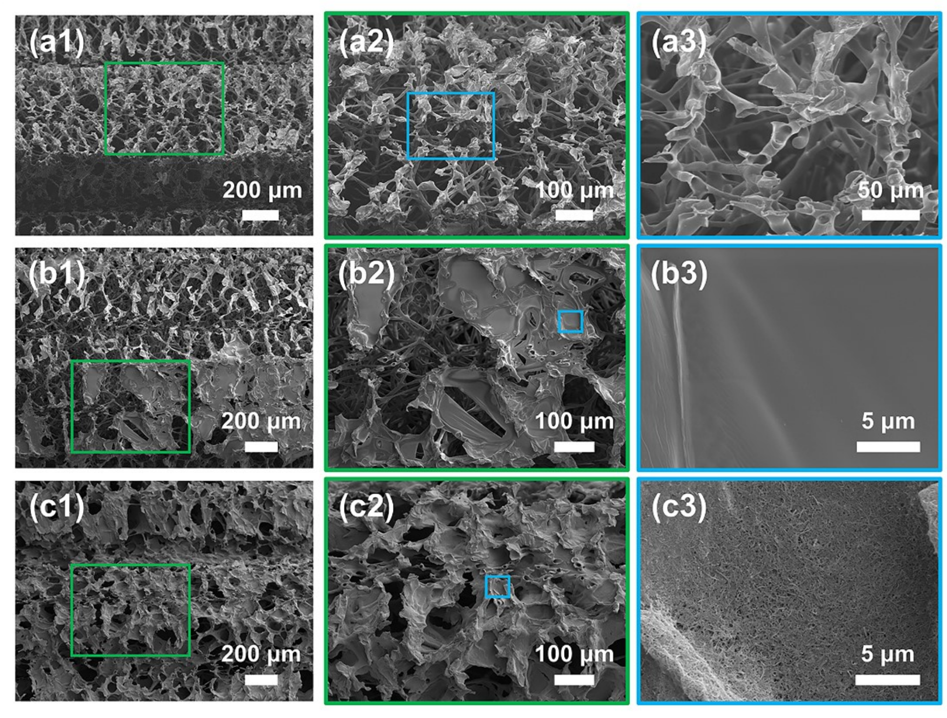

**Fig. S3** The surface view of (a) JE, (b) PJE and (c) CJE, respectively.

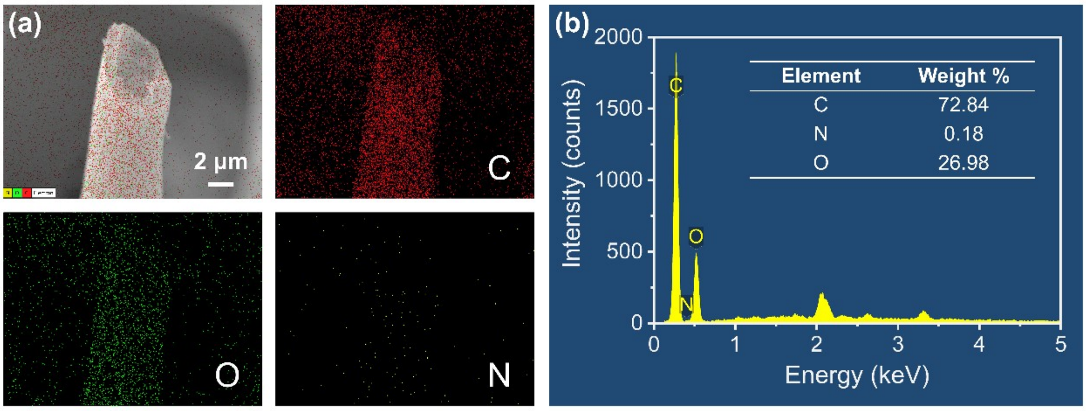

| Element | Weight % |
|---|---|
| C | 72.84 |
| N | 0.18 |
| O | 26.98 |

**Fig. S4** (a) EDS mapping images and (b) EDS spectrum of microfibre in PJE.

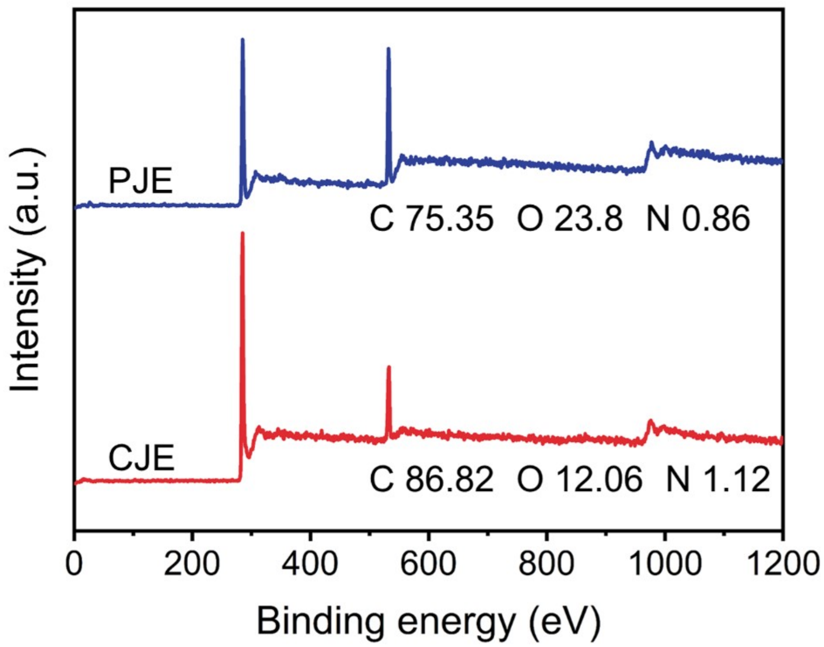

**Fig. S5** The XPS survey spectrum of PJE and CJE.

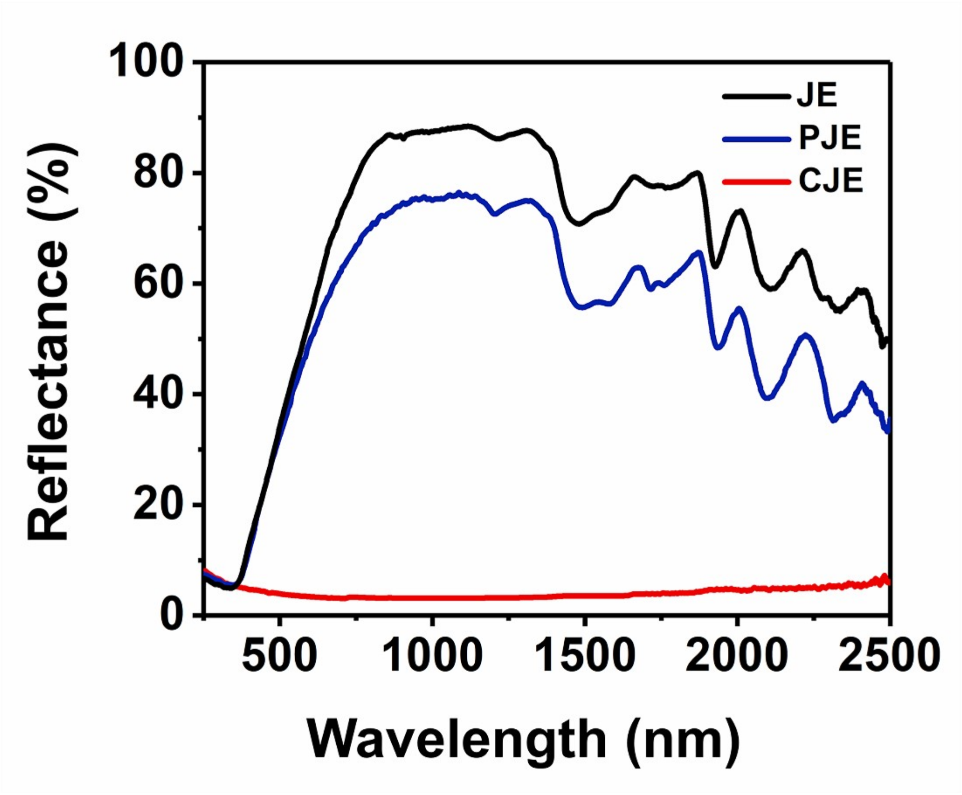

**Fig. S6** Reflectance spectra of the JE (black), PJE (blue) and CJE (red).

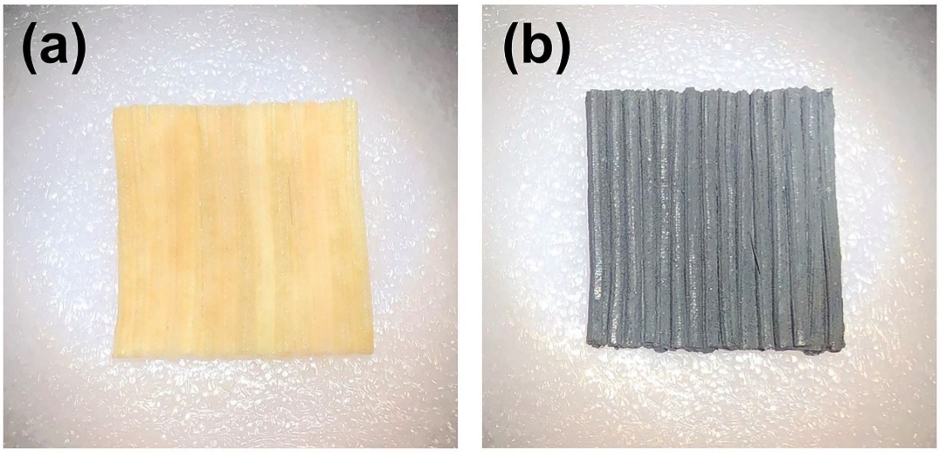

**Fig. S7** Optical photographs of (a) PJE sheet and (b) CJE sheet under simulated irradiation.

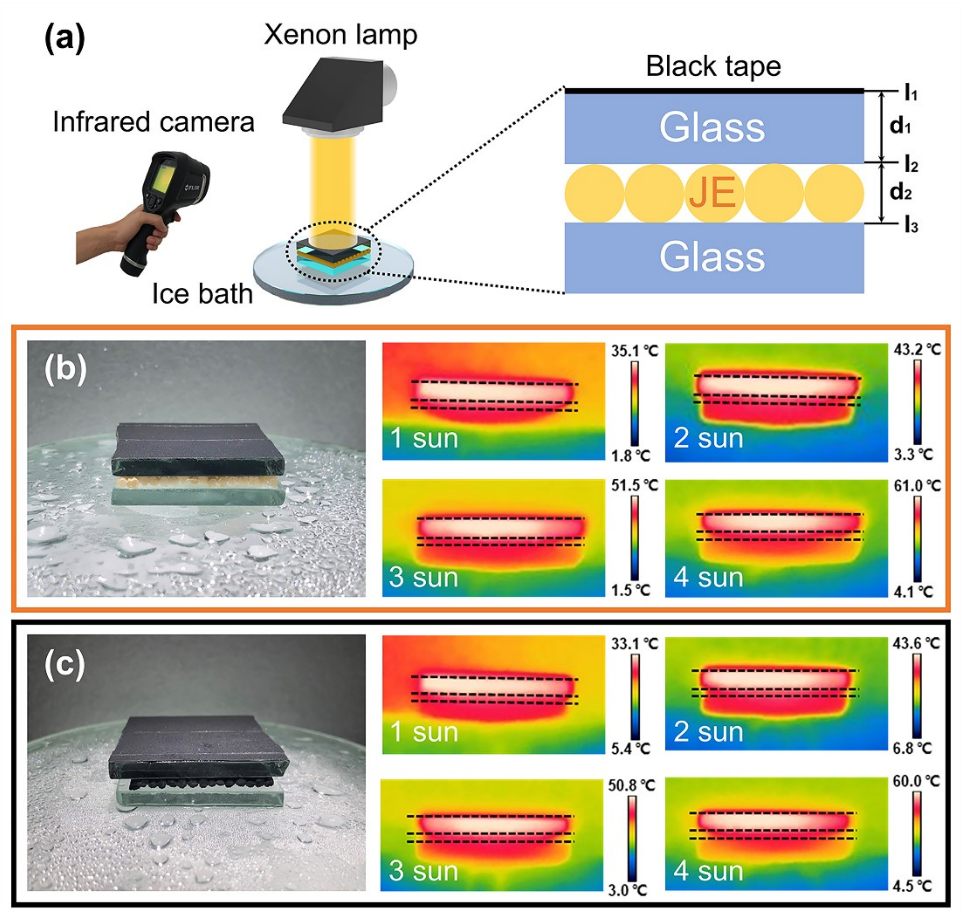

**Fig. S8** (a) Schematic diagram of the thermal conductivity measurements. IR images and photographs of (b) PJE and (c) CJE reaching thermal equilibrium under different simulated irradiation.

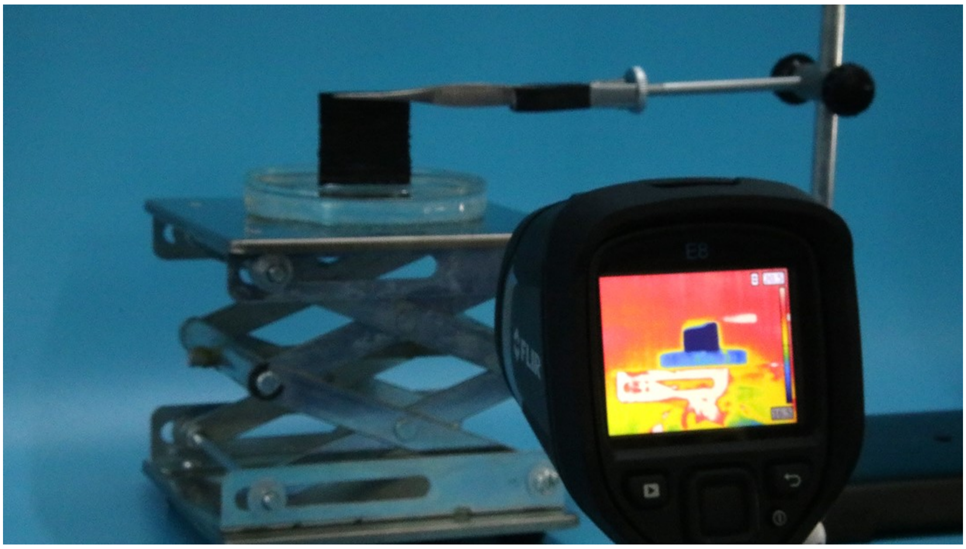

**Fig. S9** Fluid rise inside the fibre sheet was monitored using an IR camera.

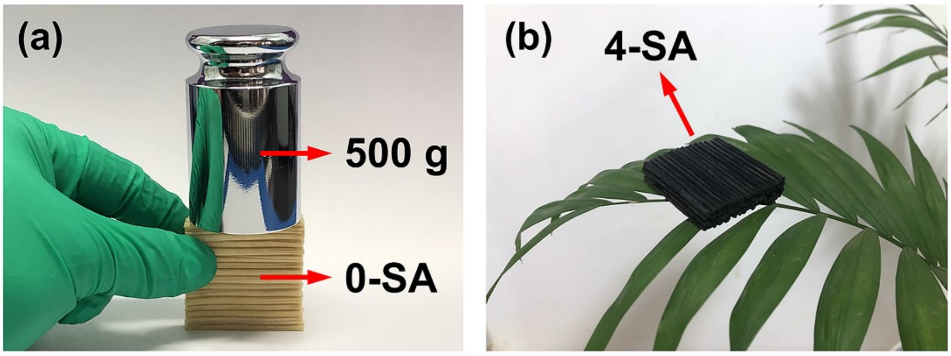

**Fig. S10** (a) 0-SA was compressed by a 500g weight. (b) 4-SA standing on the plant leaves.

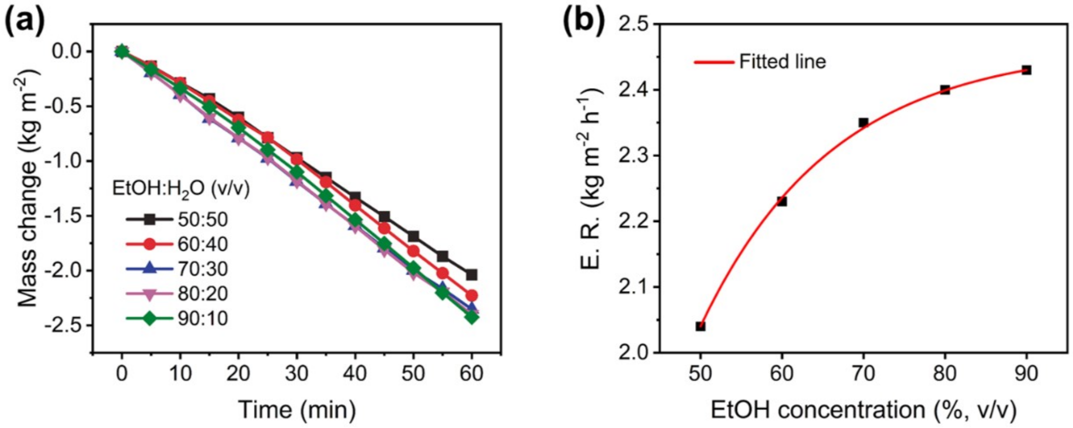

**Fig. S11** (a) Cumulative mass change and (b) evaporation rate for EtOH-$H_2O$ mixture with 1-SA versus solar light irradiation time at various concentrations.

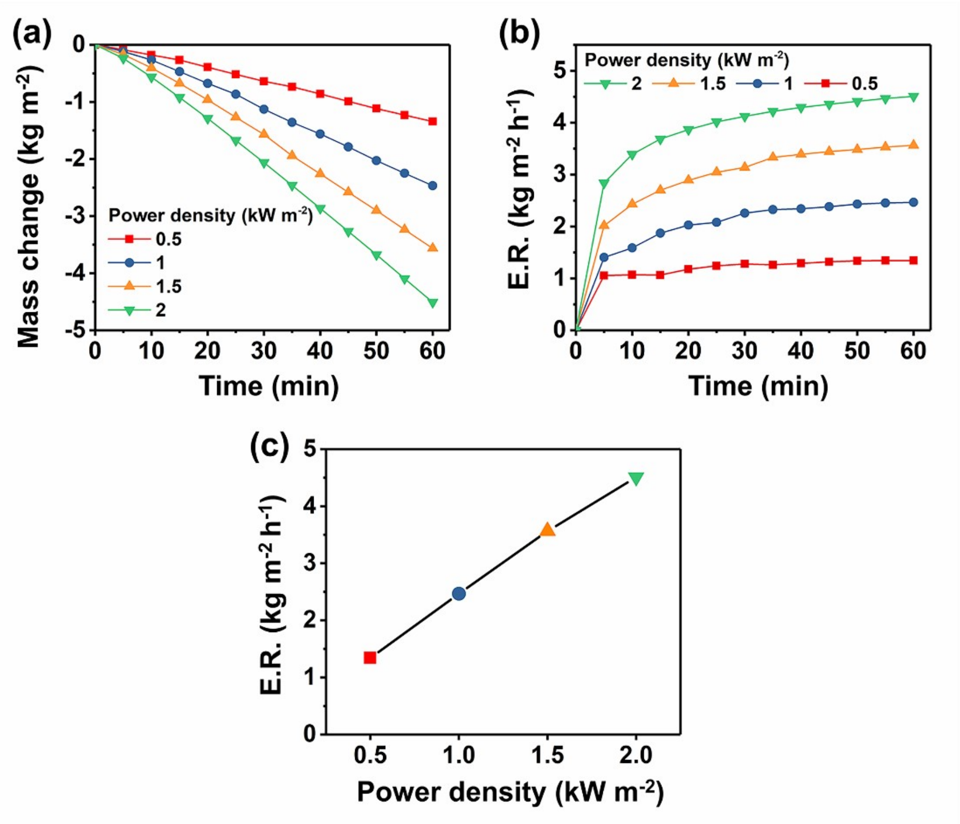

**Fig. S12** (a) Mass change and (b) evaporation rate of dye solution with EtOH-$H_2O$ system using 1-SA versus solar light irradiation time at various light power densities. (c) Stabilized evaporation rate under varied power densities.

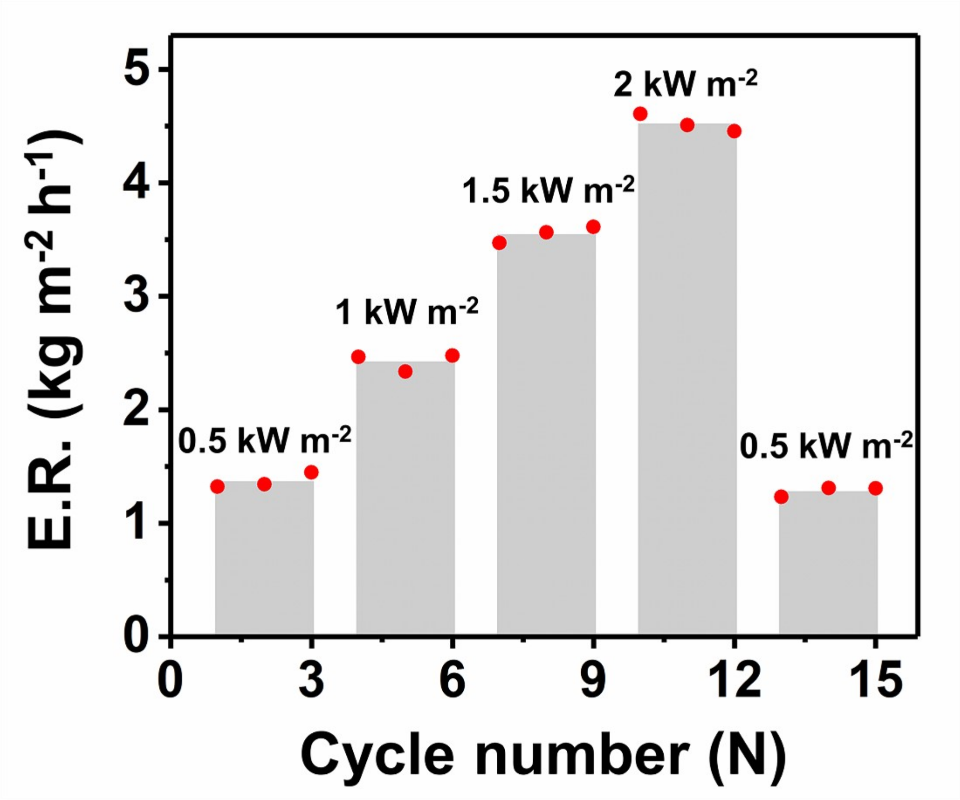

**Fig. S13** Evaporation rate versus cycle number at different solar light power densities of 1-SA.

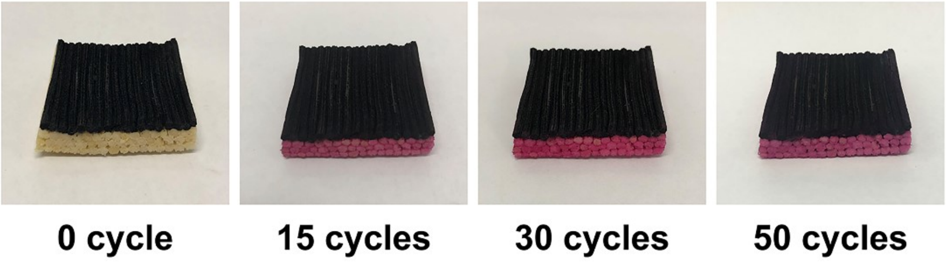

**Fig. S14** Optical photograph of 1-SA after dye wastewater purifications for 0, 15, 30, 50 cycles.

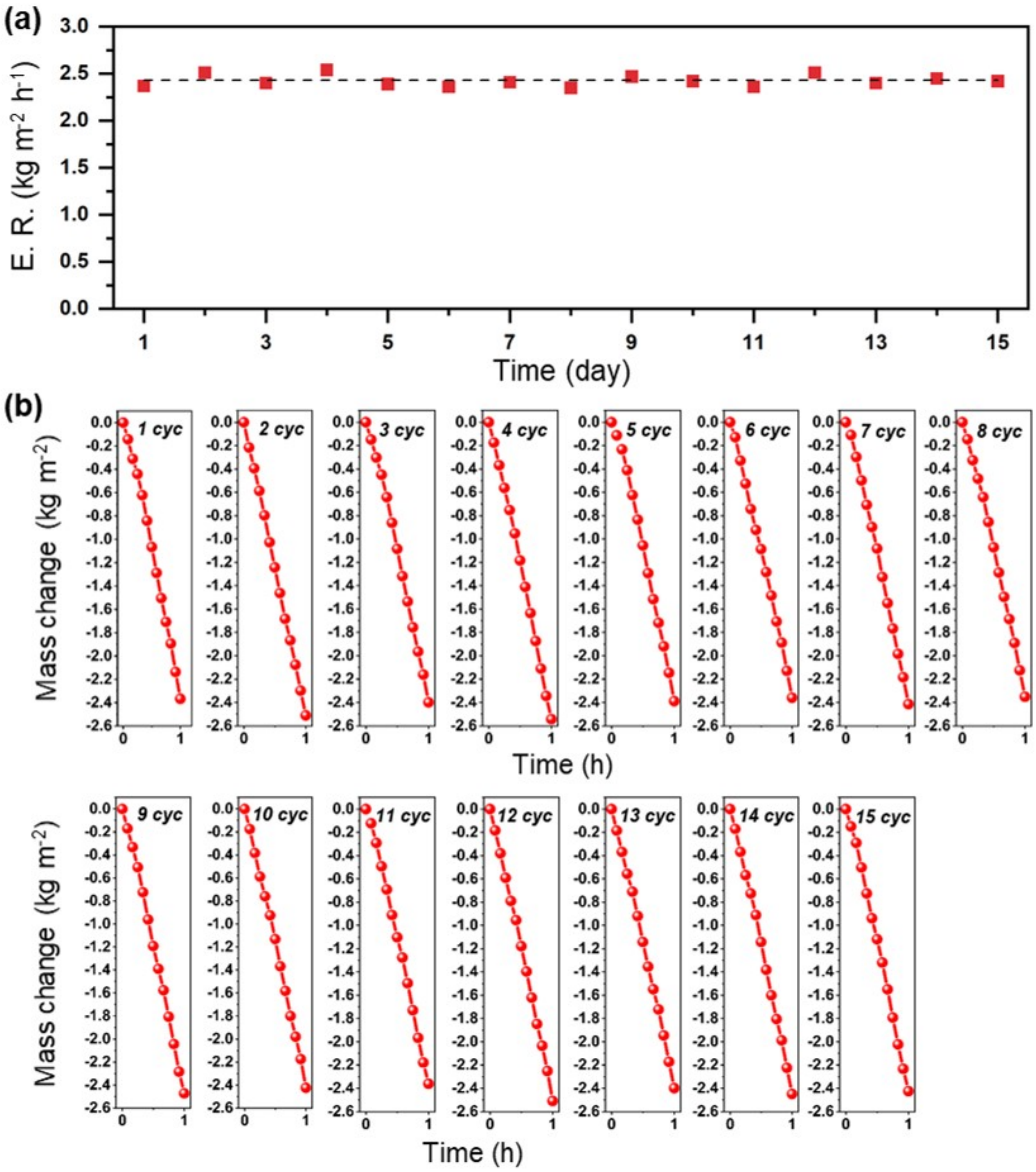

**Fig. S15** The long-time stability of the 1-SA in EtOH-$H_2O$ evaporation up to 15 days under 1 kW $m^{-2}$ solar light irradiation for 1 h everyday: (a) Evaporation rate per day and (b) corresponding detailed data.

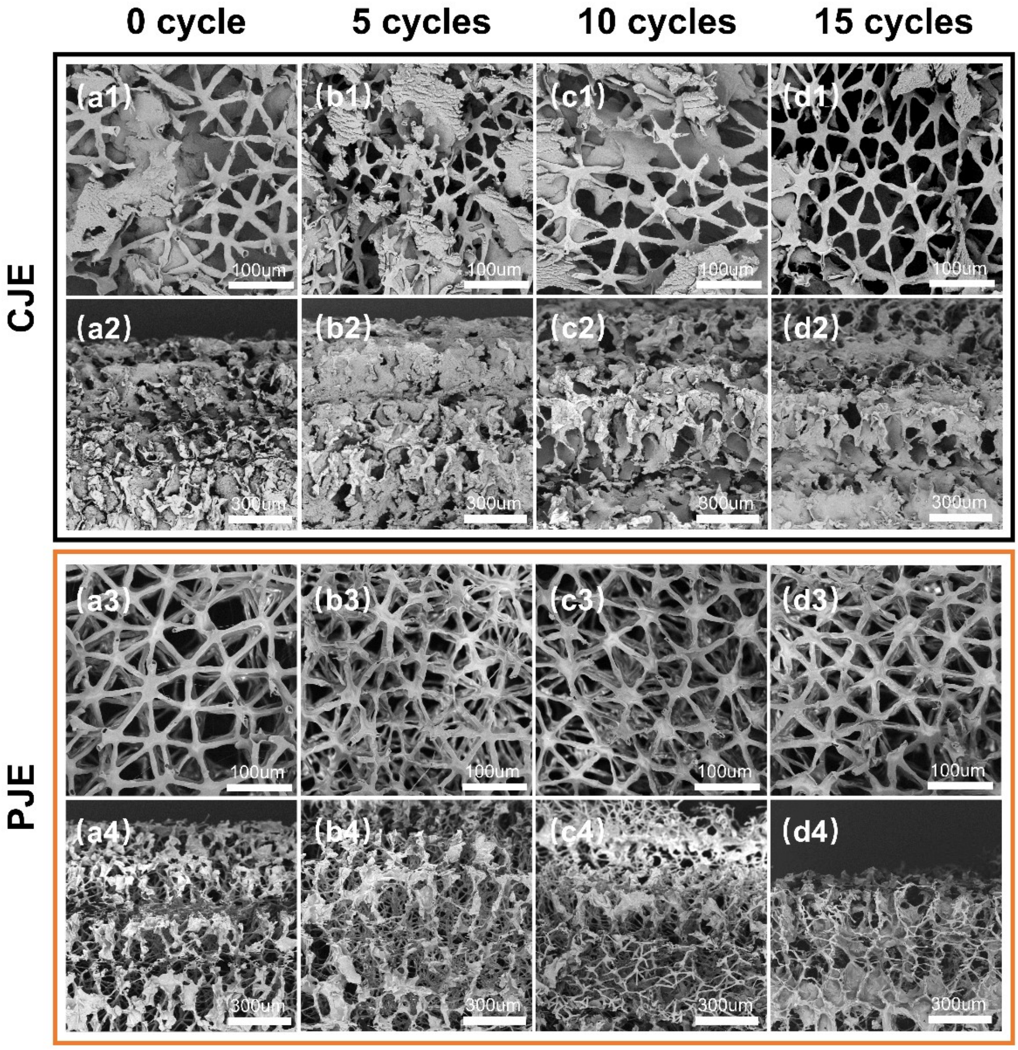

**Fig. S16** SEM images of (a1)-(d1) cross section and (a2)-(d2) longitudinal surface for CJE. SEM images of (a3)-(d3) cross section and (a4)-(d4) longitudinal surface for PJE at reuse cycles of 0, 5, 10, 15 times, respectively.

SEM images of the CJE and PJE at different recycling were detected to characterize the stability of microscopic morphology. Comparing to the original PJE and CJE, the 3D network structure of the porous 1-SA was obviously observed, and porous structure consisting of numerous skeletons remained. The surface morphologies of the sample at different cycles were rough, which were presented in SEM images, demonstrating the stability of structure during the process of reuse. Stability of 3D connected channels construction and rough structure have been proved to be a reasonable strategy to improve sunlight absorption via enhanced incident light refraction, and boost liquid transport.[10]

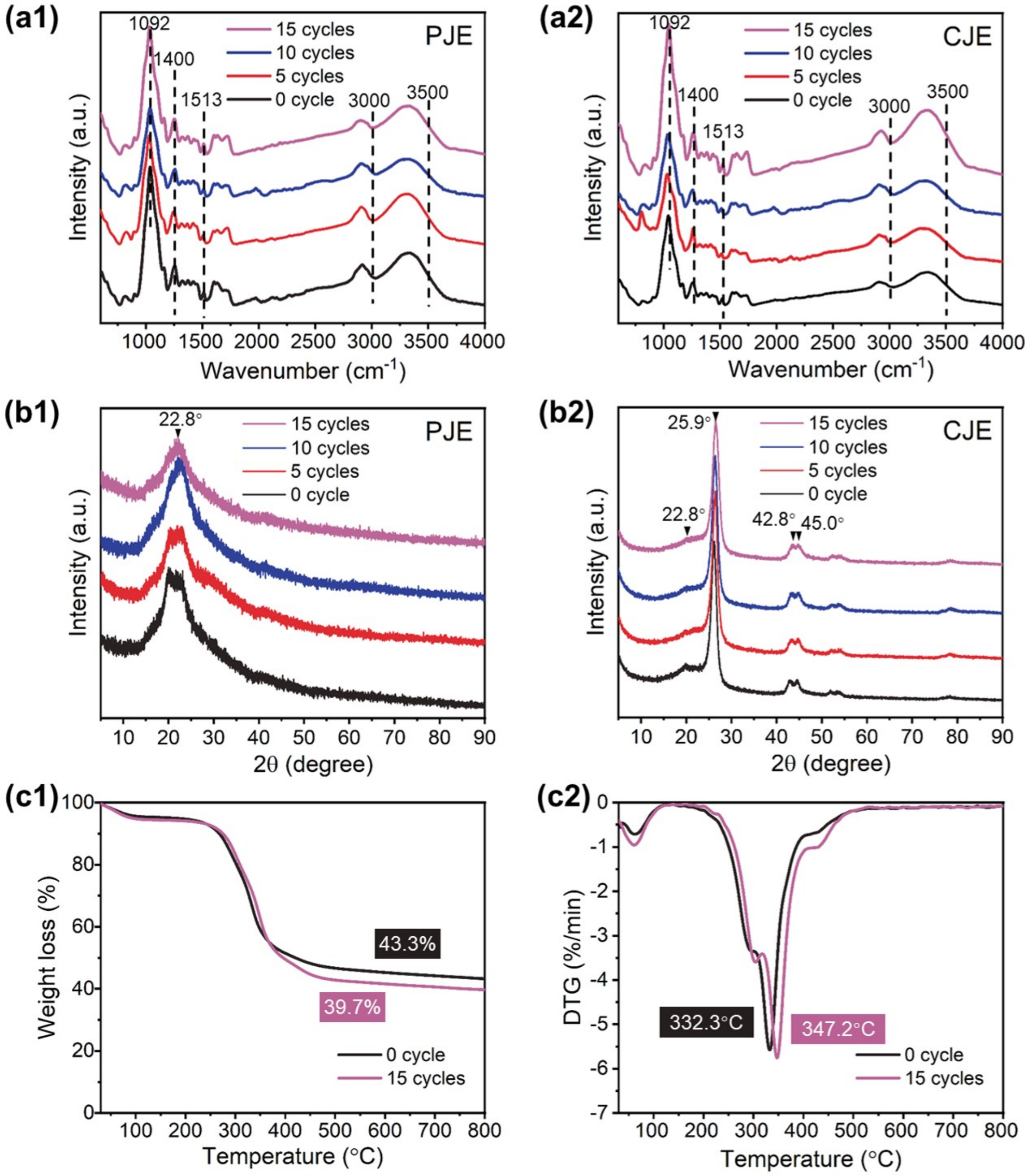

**Fig. S17** (a) FTIR spectrum of PJE and CJE for recycling 0, 5, 10, 15 times. (b2) XRD pattern of PJE and CJE for recycling 0, 5, 10, 15 times. (c1) TG and (c2) DTG curves of 1-SA for recycling 0 and 15 times.

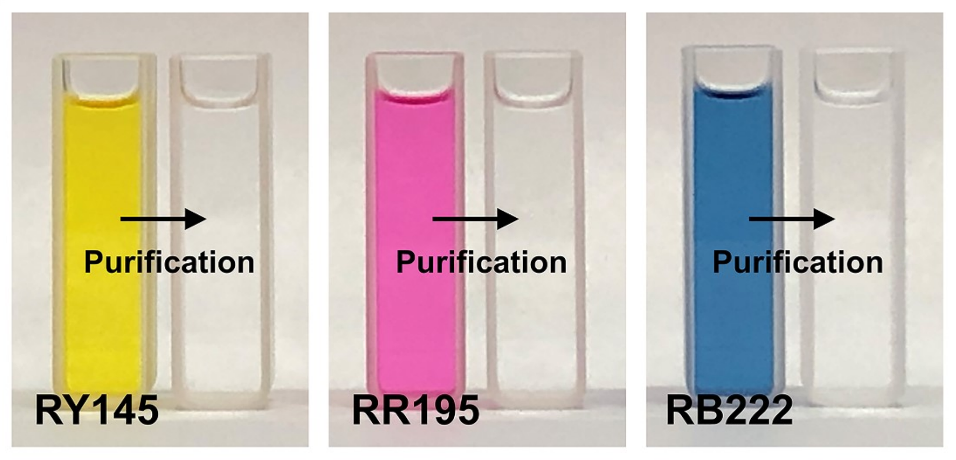

**Fig. S18** Optical images of EtOH-$H_2O$ dye solutions and corresponding condensate of various reactive dyes: RY145, RR195 and RB222.

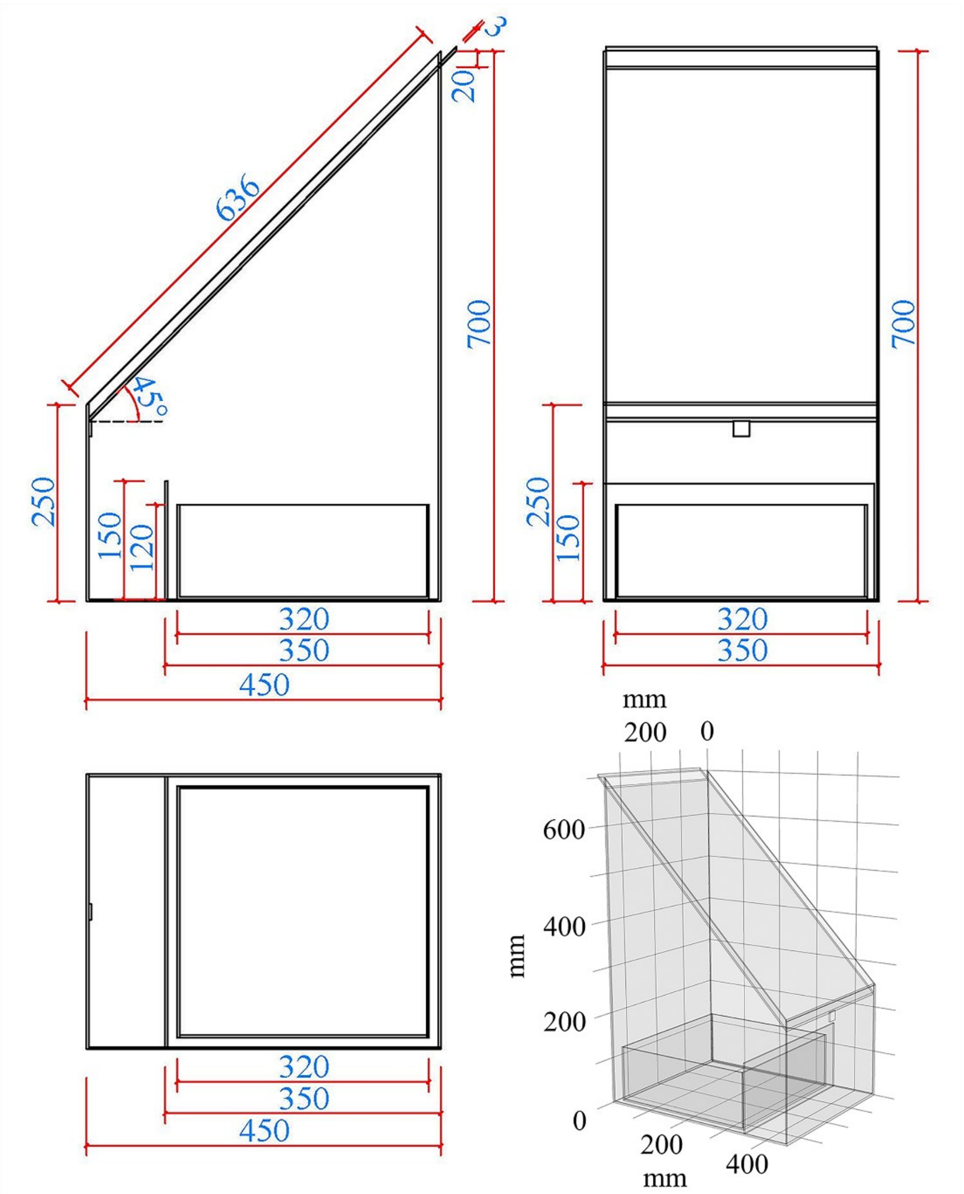

**Fig. S19** Dimensional design and 3D model of the solar still chamber. Unit: mm.

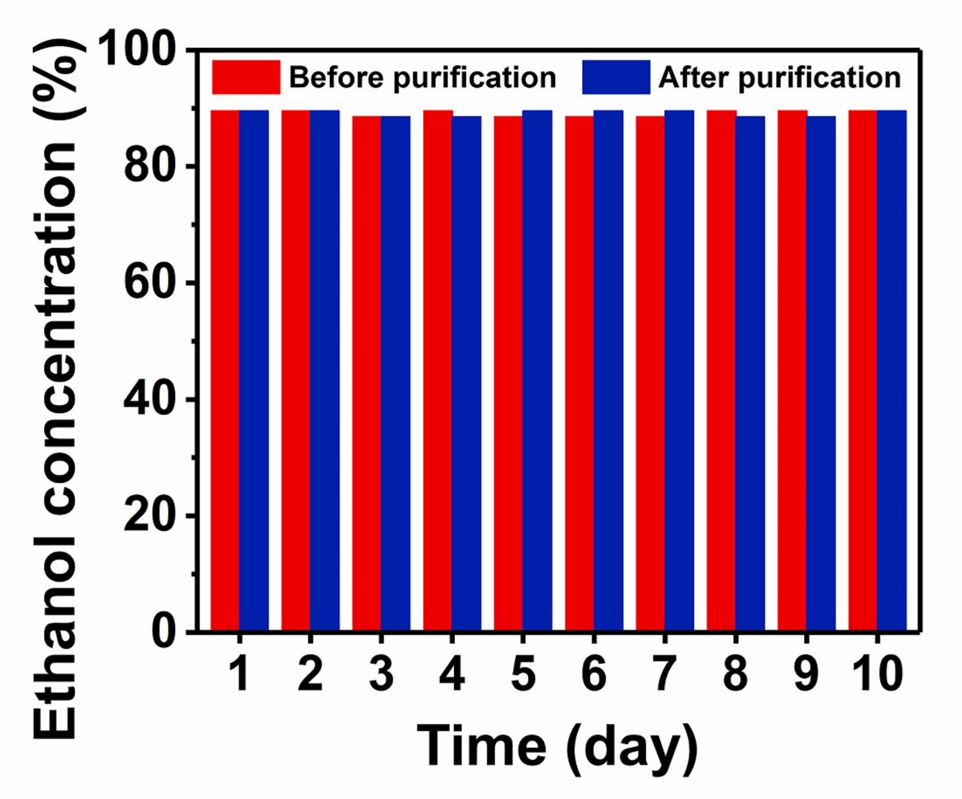

**Fig. S20** The content of ethanol in the solution before and after purification using custom-designed system.

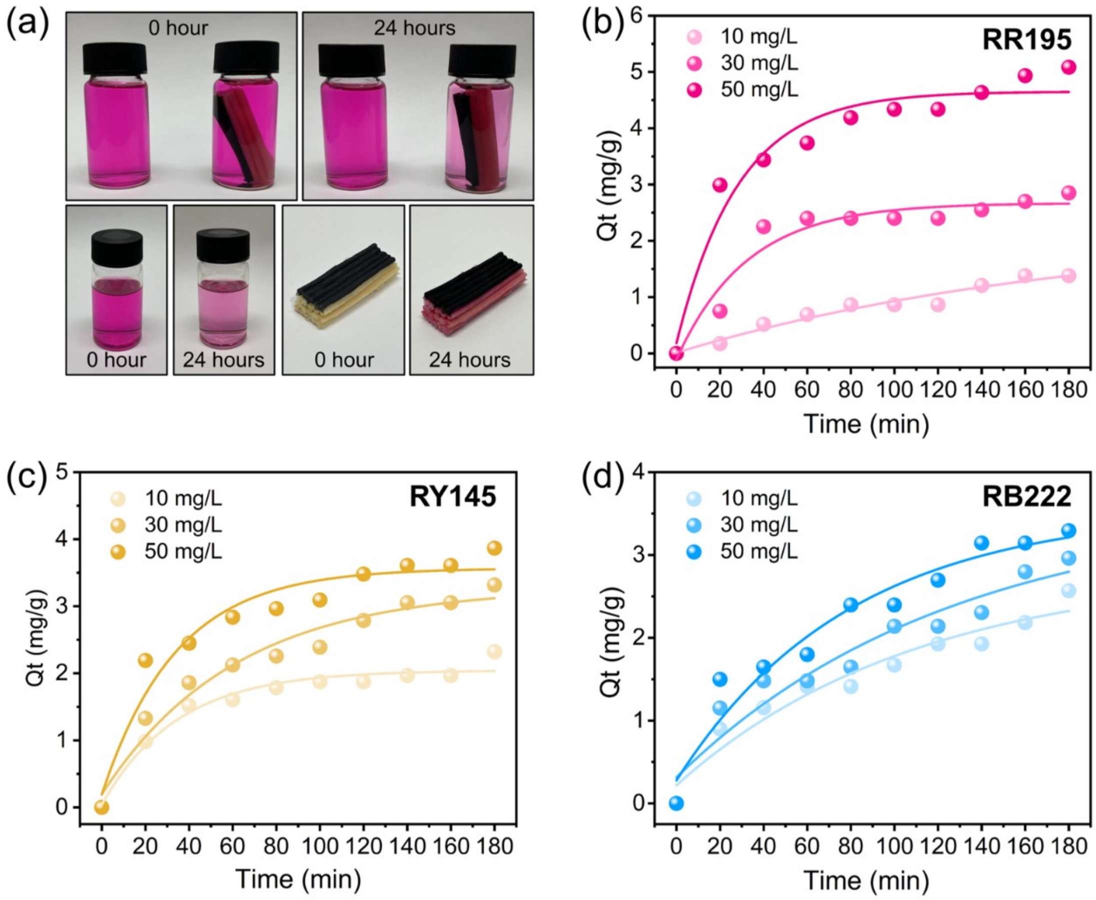

**Fig. S21** (a) Optical photograph of the RR195 dye-contaminated EtOH-$H_2O$ mixture before and after the adsorption by 1-SA. Effects of time and initial dye concentrations on the adsorption capacity of (b) RR195, (c) RY145, and (d) RB222 onto 1-SA (m = 0.2 g, V= 100 mL, $C_0$ = 10, 30, and 50 mg/L, T=30 °C).

The adsorption experiments have been performed monitoring the adsorption capacity of different dye-contaminated EtOH-$H_2O$ mixture at various initial concentration. Fig. S21a presented the optical photographs of 50 mg/L RR195 dye-contaminated EtOH-$H_2O$ mixture before and after adsorption for 24h at room temperature. The significant light color of the solution was observed. Furthermore, the effects of solution concentration on the adsorption for the investigated dye-contaminated EtOH-$H_2O$ mixture were examined, which were presented in Fig. S21b-d of RR195, RY145, and RB222 with 10, 30, and 50 mg/L for 0-180 min at 30 °C, respectively. It can be seen that all dyes exhibited adsorption onto the 1-SA during the period of monitoring at the designed concentration range. The adsorption capacities enhanced with an increase in the initial concentration, and the adsorption capacities of the dyes were sufficiently promoted when prolonged the contact time during the initial stages. Subsequently, the adsorption process slowed down until the adsorption equilibrium was tardily obtained. As illustrated in Fig. S21b-d, the maximum adsorption capacities of the 1-SA for RR195, RY145, and RB222 were 5.08, 3.86, and 3.29 mg/g at the concentration of 50mg/L, respectively. As the green cellulose materials, the natural JE fibre demonstrated adsorption performance, which promoted the purification of the dye-contaminated EtOH-$H_2O$ mixture.

**Table S1** Structural components of solar absorbers.

| Solar absorber | Amount of layers | |
|---|---|---|
| | **CJE sheet** | **PJE sheet** |
| 0-SA | 0 | 4 |
| 1-SA | 1 | 3 |
| 2-SA | 2 | 2 |
| 3-SA | 3 | 1 |
| 4-SA | 4 | 0 |

**Table S2** The mass of x-SA and the mass ratio of CNTs in it.

| Solar absorber | m (g) | Δm (g) | Mass ratio of CNTs (%) |
|---|---|---|---|
| 0-SA | 0.55 | 0 | 0 |
| 1-SA | 1.04 | 0.49 | 47.12 |
| 2-SA | 1.46 | 0.91 | 62.33 |
| 3-SA | 1.90 | 1.35 | 71.05 |
| 4-SA | 2.31 | 1.76 | 76.19 |

Note: **m** means the mass of the evaporator, **Δm** represents the difference between **m** and the mass of 1-SA, the value of **Mass ratio** is obtained by calculating the ratio of **Δm** to **m**.

**Table S3** Surface temperatures of different solar absorbers under 1 kW $m^{-2}$ condition.

| **Solar absorber** | **Temperature (0min, °C)** | | **Temperature (15min, °C)** | | **$\Delta T_{sp}$** | **$\Delta \bar{T}$** |
|---|---|---|---|---|---|---|
| | **$T_{sp1}$** | **$\bar{T}_1$** | **$T_{sp2}$** | **$\bar{T}_2$** | | |
| Blank | 22.2 | 22.3 | 23.9 | 24.1 | 1.7 | 1.8 |
| 0-SA | 21.4 | 21.5 | 29.7 | 29.9 | 8.3 | 8.4 |
| 1-SA | 20.3 | 20.4 | 37.5 | 38.1 | 17.2 | 17.7 |
| 2-SA | 24.0 | 24.0 | 40.8 | 40.6 | 16.8 | 16.6 |
| 3-SA | 23.4 | 23.4 | 39.4 | 39.3 | 16.0 | 15.9 |
| 4-SA | 22.7 | 22.9 | 38.9 | 38.9 | 16.2 | 16.0 |

Note: **$T_{sp}$** means spot temperature, **$\bar{T}$** represents the average temperature in the region and **$\Delta T$** is the difference in temperature between 0 and 15 min.

**Table S4** Data of solar purification for EtOH-$H_2O$ dyeing solution in 10 days.

| Date | weather | Wind speed ($m\ s^{-1}$) | Ambient T (°C) | Daily Insolation ($kW\ m^{-2}$) | Initial concentration of ethanol (v/v, %) | Concentration of collected ethanol (v/v, %) | Daily yield (g) |
|---|---|---|---|---|---|---|---|
| 27th, Aug., 2020 | Sunny | 1.6-3.3 | 24-33 | 0.642 | 89.5 | 89.5 | 690.8 |
| 28th, Aug., 2020 | Sunny | 1.6-3.3 | 22-34 | 0.637 | 89.5 | 89.5 | 759.3 |
| 29th, Aug., 2020 | Sunny | 0.3-3.3 | 23-34 | 0.563 | 88.5 | 88.5 | 636.3 |
| 30th, Aug., 2020 | Cloudy to sunny | 0.3-3.3 | 24-34 | 0.413 | 89.5 | 88.5 | 605.6 |
| 31th, Aug., 2020 | Cloudy to sunny | 3.4-7.9 | 26-34 | 0.533 | 88.5 | 89.5 | 585.5 |
| 1st, Sep., 2020 | Sunny | 3.4-5.4 | 24-33 | 0.466 | 88.5 | 89.5 | 499.7 |
| 2nd, Sep., 2020 | Cloudy to sunny | 1.6-3.3 | 22-34 | 0.421 | 88.5 | 89.5 | 504.7 |
| 11th, Sep., 2020 | Cloudy | 3.4-7.9 | 21-29 | 0.405 | 89.5 | 88.5 | 491.1 |
| 30th, Sep., 2020 | Sunny to cloudy | 1.6-3.3 | 18-27 | 0.437 | 89.5 | 88.5 | 507.9 |
| 8th, Oct., 2020 | Sunny to cloudy | 1.6-3.3 | 14-22 | 0.613 | 89.5 | 89.5 | 491.4 |
| **Average** | | | **26.6** | **0.513** | **89.1** | **89.1** | **558.2** |

Note 1: The initial concentration of ethanol was obtained by measuring the dye sample, and the concentration of collected ethanol was determined by testing the condensed clean liquid.

Note 2: Data on wind speed and ambient temperature were from the China Meteorological Information Center (http://data.cma.cn).

## References

1 L. Xia, A. Wang, C. Zhang, Y. Liu, H. Guo, C. Ding, Y. Wang and W. Xu, *Green Chem.*, 2018, **20**, 4473-4483. DOI: 10.1039/c8gc01814f

2 L. Xia, A. Wang, Y. Wang, C. Zhang, Y. Wang, S. Zhou, Z. Fu, H. Zhao, C. Ding and W. Xu, *Green Chem.*, 2021, **23**, 796-807. DOI: 10.1039/d0gc02839h

3 X. Fan, Y. Yang, X. Shi, Y. Liu, H. Li, J. Liang and Y. Chen, *Adv. Funct. Mater.*, 2020, **30**, 2007110. DOI: 10.1002/adfm.202007110

4 T. Lin, C. Yang, Z. Wang, H. Yin, X. Lü, F. Huang, J. Lin, X. Xie and M. Jiang, *Energ. Environ. Sci.*, 2014, **7**, 967-972. DOI: 10.1039/c3ee42708k

5 Y. Xu, C. Tang, J. Ma, D. Liu, D. Qi, S. You, F. Cui, Y. Wei and W. Wang, *Environ. Sci. Technol.*, 2020, **54**, 5150-5158. DOI: 10.1021/acs.est.9b06072

6 Q. Jiang, L. Tian, K. K. Liu, S. Tadepalli, R. Raliya, P. Biswas, R. R. Naik and S. Singamaneni, *Adv. Mater.*, 2016, **28**, 9400-9407. DOI: 10.1002/adma.201601819

7 C. Chen, Y. Li, J. Song, Z. Yang, Y. Kuang, E. Hitz, C. Jia, A. Gong, F. Jiang, J. Y. Zhu, B. Yang, J. Xie and L. Hu, *Adv. Mater.*, 2017, **29**, 1701756. DOI: 10.1002/adma.201701756

8 T. Li, M. Zhu, Z. Yang, J. Song, J. Dai, Y. Yao, W. Luo, G. Pastel, B. Yang and L. Hu, *Adv. Energy. Mater.*, 2016, **6**, 1601122. DOI: 10.1002/aenm.201601122

9 X. Wang, T. Zhan, Y. Liu, J. Shi, B. Pan, Y. Zhang, L. Cai and S. Shi, *ChemSusChem*, 2018, **11**, 4086-4093. DOI: 10.1002/cssc.201801826

10 K. Sun, H. Cui, R. Xu, L. Wang, M. Li, Z. Yang, M. Zhao and N. Wei, *Sol. Energy Mater. Sol. Cells*, 2022, **240**, 111722. DOI: 10.1016/j.solmat.2022.111722